Indian Journal of Pure & Applied Physics
Vol. 64, June 2026, pp. 600-611
DOI: 10.56042/ijpap.v64i6.16691

# Thermohydrodynamic Behavior of Nonlinear Slip Flow of Ternary Hybrid Nanofluid in Low and High Porosity Porous-Media: Applied to Packed Bed of Small Particles and Metal Foam

B S Kamilla[a], S Shaw[b], D N Thatoi[a] & M K Nayak[c*]

[a]Department of Mechanical Engineering, ITER, Siksha 'O' Anusandhan Deemed to be University, Bhubaneswar 751 030, India

[b]Department of Mathematics and Statistical Sciences, Botswana International University of Science and Technology, Private Bag 16, Palapye, Botswana

[c]Department of Applied Sciences, National Institute of Technology Delhi, Delhi 110 036, India

*Received: 17th February 2025; accepted: 5th May 2026*

The present study aims at exploring thermohydrodynamic behavior of nonlinear slip flow of Ag + $Al_2O_3$ + Graphene +Water ternary hybrid nanofluid (THNF) in porous media, with applications to packed beds and metal foams. The motivation of this study to achieve a significant enhancement in thermal efficiency and heat transfer rates (HTRs) for advanced engineering applications. Compared to mono and binary nanofluids, these nanofluids provide better heat regulation and greater thermal conductivity by mixing Ag,$Al_2O_3$, graphene nanoparticles in a base fluid. Because it provides better heat transfer and flow stability than traditional fluids and binary hybrid nanofluids, this work is important for the design of high-efficiency thermal management systems. A 3D solution of transformed governing equations is obtained by using Galerk in finite element method. Fluid velocity $f'(\eta)$ increases with rise in curvature parameter $\Omega$ while it whittles down with rise in slip parameter $\gamma$ at low Reynolds number subject to uniform and linear heating in low porosity porous media (packed bed of small particles) and high porosity porous media (metal foam). Further, fluid temperature $\theta(\eta)$ for THNF is greater than that of hybrid nanofluid (HNF) in both boundary heating subject to both type of porous media.

**Keywords:** Ternary hybrid nanofluid, Low and high porosity porous media, Modified darcy number, Modified grash of number, Modified thompson, Troian nonlinear slip

## 1 Introduction

By distributing nanoscale particles (usually metallic, metal-oxide, or carbon-based compounds, 1-100 nm) into traditional heat transfer base fluids like water, ethylene glycol, or oil-engineered colloidal suspensions-known as nanofluids are produced. They are made to improve heat transmission in industrial settings, overcoming the low thermal conductivity constraints of traditional coolants[1-3]. Nanofluids are utilized in industries that need smaller components and high-efficiency heat removal. These include electronics cooling, machining and lubrication, automobile radiators, solar energy collection, and biomedical applications[4].

Despite their benefits, a number of obstacles still stand in the way of their widespread industrial adoption, such as instability and sedimentation, high production costs, increased viscosity/pressure drop, and erosion and fouling[5,6]. Two different kinds of nanoparticles (such as metals, metal oxides, or carbon-based compounds) are suspended into a base fluid to create hybrid nanofluids (HNFs). Ternary hybrid nanofluids (THNFs) represent a more advanced, recent invention where three distinct solid nanoparticles are evenly distributed in a base fluid. They exhibit "synergistic effect" due to their high conductivity, stability/corrosion resistance, surface area/lightweight. Advanced electronics cooling, renewable energy storage, biomedical devices, industrial processes, and automotive cooling are crucial applications of HNFs/THNFs[7]. Many researchers worked in the related aspects. For instance, studied rotational flow and thermal behavior of ternary hybrid nanomaterials at small and high Prandtl numbers[8]. In order to study thermo-solutal convection of a ternary nanofluid with diffusive blocks and non-linear radiative effects. A comparison of graphene, copper, and ferrous sulfate nanoparticles

*Corresponding author: E-mail: manojknayak@nitdelhi.ac.in

in radiative nanofluid flow over a porous curved cylinder was studied[9]. According to their findings, skin friction and heat transfer rates were significantly enhanced by raising the power-law index because of increased convective acceleration.

Recent studies describe complicated systems such as metal foams and packed beds, addressing flow in both low and high porosity media. These systems are essential for maximizing temperature control in solar energy collectors, electronics, and car cooling systems. In order to manage flow and improve energy transfer in industrial processes, the Darcy-Forchheimer model is used to examine inertial forces on high-speed flows in porous media[10]. Some of them are highlighted in the present section. For instance, Heat transfer in a HNF flow in porous media was one of the transport and thermodynamic processes in multiphysics systems that was investigated[11]. Investigated a machine learning-based Bayesian regularization approach for thermal analysis of tri-hybrid nanofluid flow on a stretched sheet[12]. Their findings showed that while a higher volume fraction of nanoparticles reinforced thermal boundary layers, an increased magnetic field and porosity reduced the flow velocity.

The partial slip condition may be linear or non-linear nature depending upon the low/high flow rate situations associated with the thermal systems. Optimizing heat transfer in microfluidic applications requires a more realistic simulation of fluid behaviour at the solid interface, which is made possible by taking nonlinear slip boundary conditions into account in fluid flow issues. In view of its vital role in different sectors, many researchers have studied the flow analysis in association with partial slip conditions. As illustration, influence of Thompson and Troian slip on the nanofluid flow past a permeable plate was studied[13]. The same effects on THNF over a permeable plate were investigated[14]. The effect was further studied on CNT-$Fe_3O_4$/kerosene oil HNF flow over an exponential stretching sheet[15]. It was observed that heat transfer (HT) rate was enhanced by 30.11% on elevating the volume fraction of $Fe_3O_4$ from 1% to 10%.

Till date, very few studies have been carried out regarding the boundary layer flow and HT behavior of THNFs over stretched surfaces of different geometries. However, the non-linear slip flow and HT behavior of THNF over stretched cylinder embedded in a Darcy medium and non-Darcy medium with low and high porosity subject to uniform and linear boundary heating conditions at low Reynolds number are yet to be investigated.

The novelties of the present study are as follows:

i. Consideration of low porosity porous medium as packed bed of small particles and high porosity porous medium as metal foam.
ii. Low Reynolds numbers are taken into consideration.
iii. Thermal behavior of Ag + $Al_2O_3$ + *Graphene* +*Water* THNF flow over a stretched cylinder subject to uniform and linear boundary heating conditions are carried out.
iv. Modified Thompson and Troian nonlinear slip model is adopted.

In the present study the justification of introduction of packed bed of small particles is that the flow of THNF optimizes heat transfer in nuclear and chemical reactors. Further, introduction of metal foam with the flow of THNF provides high-strength, low-weight alternatives for heat dissipation in high-power electronic devices.

## 2 Mathematical Description and the Physical Model

The non-linear slip flow and thermal behavior of $Ag + Al_2O_3 + Graphene + Water$ THNF over a stretched cylinder in low porosity porous medium (packed bed of small particles) and high porosity porous medium (metal foam) subject to uniform and linear boundary heating conditions are considered as shown in Figs. 1 and 2 respectively. In the present study, it is assumed that water is base fluid; silver, aluminum oxide, and graphene are nanoparticles. Here water is considered because of its low viscosity, low density, and better heat propagation. Further, silver is used as a nanoparticle due to its better thermal conductivity and hydrophilic characteristic; aluminum oxide is used as a nanoparticle due to its better stability so as avoid sedimentation; graphene is used as a nanoparticle due to its extremely high thermal conductivity. As a consequence, a homogeneous and stable THNF is developed.

The assumptions of the problem are:

i. The flow is steady, laminar and incompressible.
ii. The base fluid as water and nanoparticles namely silver, aluminum oxide, and graphene are in thermal equilibrium.
iii. The stretched cylinder is embedded in low porosity porous media (packed bed of small particles) and high porosity porous media (metal foam).

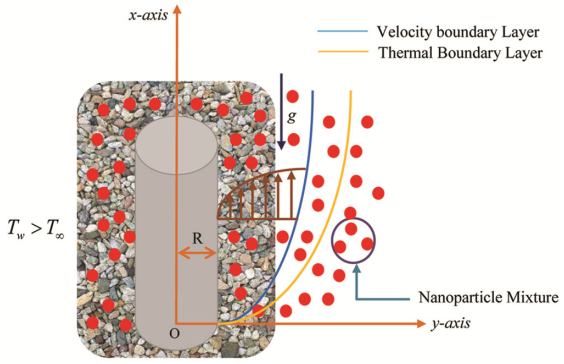


Fig. 1 — Flow geometry for stretched cylinder embedded in low porosity porous media (packed bed of small particles)

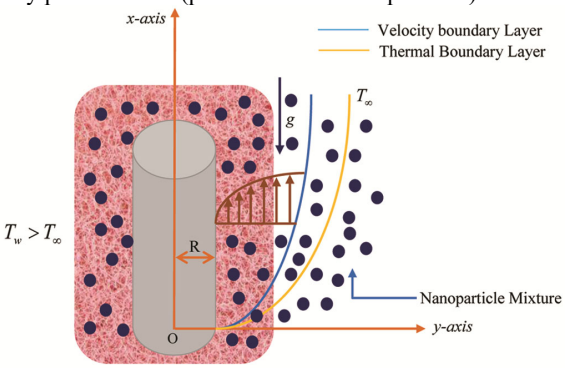


Fig. 2 — Flow geometry for stretched cylinder embedded in high porosity porous media (metal foam)

iv. Gravity induced buoyancy flow is introduced.
v. Heat transportations are boosted by thermal radiation and viscous dissipation.
vi. Modified Thompson and Troian non-linear slip model has been chosen.
vii. Uniform and linear heating conditions are adopted.
viii. Low Reynolds numbers are taken into consideration.

Taking the above assumptions into consideration and invoking the Boussinesq theory, the requisite governing equations are[16,17]

### 2.1 Governing Equations

#### *2.1.1 Continuity Equation*

$$\frac{\partial(ru)}{\partial x}+\frac{\partial(rv)}{\partial r}=0 \qquad \ldots (1)$$

### 2.2 Low Porosity Porous Media (Packed Bed of Small Particles)

#### *2.2.1 Momentum equation*

$$\frac{\rho_{THNF}}{\varepsilon^2}\left(u\frac{\partial u}{\partial x}+v\frac{\partial u}{\partial r}\right)=\frac{\mu_{THNF}}{\varepsilon}\left(\frac{\partial^2 u}{\partial r^2}+\frac{1}{r}\frac{\partial u}{\partial r}\right)+ g\rho_{THNF}\beta_{THNF}\left(T-T_\infty\right)-\frac{\mu_{THNF}u}{K}$$

… (2 (a))

#### *2.2.2 Energy equation*

$$u\frac{\partial T}{\partial x}+v\frac{\partial T}{\partial r}=\left\{\frac{k_{THNF}}{\left(\rho c_p\right)_{THNF}}+\frac{16\sigma^* T_\infty^3}{3k^*\left(\rho c_p\right)_{THNF}}\right\}\left(\frac{\partial^2 T}{\partial r^2}+\frac{1}{r}\frac{\partial T}{\partial r}\right)+\frac{\mu_{THNF}}{\left(\rho c_p\right)_{THNF}}\left(\frac{\partial u}{\partial r}\right)^2+\frac{\mu_{THNF}}{\left(\rho c_p\right)_{THNF}}\frac{u^2}{K}$$

... (2 (b))

### 2.3 High Porosity Porous Media (Metal Foam)

#### *2.3.1 Momentum Equation*

$$\frac{\rho_{THNF}}{\varepsilon^2}\left(u\frac{\partial u}{\partial x}+v\frac{\partial u}{\partial r}\right)=\frac{\mu_{THNF}}{\varepsilon}\left(\frac{\partial^2 u}{\partial r^2}+\frac{1}{r}\frac{\partial u}{\partial r}\right)+g\rho_{THNF}\beta_{THNF}\left(T-T_\infty\right)-\frac{\mu_{THNF}u}{K}-\rho_{THNF}Fu^2$$

… (3 (a))

#### *2.3.2 Energy equation*

$$u\frac{\partial T}{\partial x}+v\frac{\partial T}{\partial r}=\left\{\frac{k_{THNF}}{\left(\rho c_p\right)_{THNF}}+\frac{16\sigma^* T_\infty^3}{3k^*\left(\rho c_p\right)_{THNF}}\right\}\left(\frac{\partial^2 T}{\partial r^2}+\frac{1}{r}\frac{\partial T}{\partial r}\right)+\frac{\mu_{THNF}}{\left(\rho c_p\right)_{THNF}}\left(\frac{\partial u}{\partial r}\right)^2+\frac{\mu_{THNF}}{\left(\rho c_p\right)_{THNF}}\frac{u^2}{K}+\frac{\rho_{THNF}F}{\left(\rho c_p\right)_{THNF}}u^3$$

… (3 (b))

### 2.4 Boundary Conditions

#### *2.4.1 Non-linear Slip cum Uniform Heating Condition*[18]

$$\left.\begin{aligned} u=U_w(x)=\frac{xU_0}{l}+\underbrace{\frac{\gamma^*\left\{r\frac{\partial}{\partial r}\left(\frac{u}{r}\right)\right\}}{\left[1-\delta^* r\frac{\partial}{\partial r}\left(\frac{u}{r}\right)\right]^{\frac{1}{2}}}}_{\text{Modified Thompson \& Troian Slip}}, \\ v=0,\quad T=T_w \quad at \quad r=a \\ u\to 0,\ T\to T_\infty \qquad as\ r\to\infty \end{aligned}\right\} \qquad \ldots (4)$$

#### 2.4.2 *Non-linear Slip cum Linear Heating Condition*[18]

$$\left.\begin{aligned} u=U_w(x)=\frac{xU_0}{l}+\underbrace{\frac{\gamma^*\left\{r\frac{\partial}{\partial r}\left(\frac{u}{r}\right)\right\}}{\left[1-\delta^* r\frac{\partial}{\partial r}\left(\frac{u}{r}\right)\right]^{\frac{1}{2}}}}_{\text{Modified Thompson \& Troian Slip}}, \\ v=0,\quad T=T_w(x)=T_\infty+Ex \quad at \quad r=a \\ u\to 0,\ T\to T_\infty \qquad as\ r\to\infty \end{aligned}\right\}$$

... (5)

Here, $(u,v)$ are velocity components in axial and radial directions respectively, $\mu_{THNF},\rho_{THNF},(\rho\beta)_{THNF},(\rho C_p)_{THNF}$ are respectively dynamic viscosity, density, coefficient

of thermal expansion and specific heat capacity of THNF, $g$ is gravitational acceleration, $U_0$ is reference velocity and $l$is reference length, $F$ is inertia coefficient, $K$ is permeability of porous medium, $\sigma^*$ is Stefan-Boltzmann constant, and $k^*$ is mean absorption coefficient, $T, T_w, T_\infty$ are temperature within boundary layer, on solid wall and ambient fluid, $E$ is the modified temperature, $\gamma^*$ is inverse critical shear rate $\left(s^{-1}\right)$ and $\delta^*$ is critical shear rate.

The fluid behaviour at the boundary between the open-cell foam and a clear fluid zone cannot be adequately described by the standard no-slip boundary condition, which justifies the employment of a non-linear slip model in high-porosity porous media, such metal foams. The fluid in high-porosity metal foams does not adhere to the boundary, especially in the interface where a clear fluid channel and the porous structure meet. Significant fluid motion occurs close to the boundary due to high permeability and large pore diameters, requiring a "slip" condition that is frequently non-linear to account for strong inertial effects. Furthermore, a "roughness-based" non-linear slip is justified since the surface roughness at the pore scale renders the traditional continuum no-slip condition inaccurate. Furthermore, non-linear slip models-which offer greater accuracy than conventional linear slip or no-slip assumptions-are crucial for effectively modelling the non-Darcy behaviours of high-velocity, high-porosity metal foams.

### 2.5 Thermophysical properties of THNF

The density of THNF[19,20],

$$\rho_{THNF} = \phi_1\rho_1 + \phi_2\rho_2 + \phi_3\rho_3 + \left(1-\phi_1-\phi_2-\phi_3\right)\rho_f \quad \ldots (6)$$

where $\rho_1, \rho_2, \rho_3$ are densities, $\phi_1, \phi_2, \phi_3$ are volume fractions of 1st , 2nd and 3rd nano particles respectively, $\rho_f$ is density of base fluid.

The specific heat capacity (SHC) of THNF,

$$\left(\rho C_p\right)_{THNF} = \phi_1\left(\rho C_p\right)_1 + \phi_2\left(\rho C_p\right)_2 + \phi_3\left(\rho C_p\right)_3 + \left(1-\phi_1-\phi_2-\phi_3\right)\left(\rho C_p\right)_f \quad \ldots (7\text{ (a)})$$

where $\left(\rho C_p\right)_1, \left(\rho C_p\right)_2, \left(\rho C_p\right)_3$ are SHCs of 1st, 2nd and 3rd nanoparticles respectively, and $\left(\rho C_p\right)_f$ is SHC of base fluid.

The thermal expansion coefficient (TEC) of THNF[21,22],

$$\left(\rho\beta\right)_{THNF} = \phi_1\left(\rho\beta\right)_1 + \phi_2\left(\rho\beta\right)_2 + \phi_3\left(\rho\beta\right)_3 + \left(1-\phi_1-\phi_2-\phi_3\right)\left(\rho\beta\right)_f \quad \ldots (7\text{ (b)})$$

where $\beta_1, \beta_2, \beta_3$ are TEC of 1st, 2nd and 3rd nanoparticles respectively, and $\beta_f$ is TEC of base fluid.

The dynamic viscosity of THNF[19,20],

$$\mu_{THNF} = \left(\phi_1\mu_{nf,1} + \phi_2\mu_{nf,2} + \phi_3\mu_{nf,3}\right)/\phi \quad \ldots (8)$$

where $\mu_{nf,1}, \mu_{nf,2}, \mu_{nf,3}$ are dynamic viscosities of 1st, 2nd and 3rd nanoparticles respectively.

The thermal conductivity (TC) of THNF[19,20],

$$k_{THNF} = \left(\phi_1 k_{nf,1} + \phi_2 k_{nf,2} + \phi_3 k_{nf,3}\right)/\phi \quad \ldots (9)$$

where $k_{nf,1}, k_{nf,2}, k_{nf,3}$ are TCs of 1st, 2nd and 3rd nano particles respectively. Here, $\phi = \phi_1 + \phi_2 + \phi_3$ is the total volume fraction.

For ith nano particle suspension (of given shape)[19,20],

$$\mu_{nf,i} = \mu_f\left(1 + B_i\phi + C_i\phi^2\right) \quad \ldots (10)$$

$$\frac{k_{nf,i}}{k_f} = \frac{k_{p,i} + \left(m_i-1\right)k_f + \left(m_i-1\right)\phi\left(k_{p,i}-k_f\right)}{k_{p,i} + \left(m_i-1\right)k_f - \phi\left(k_{p,i}-k_f\right)} \quad \ldots (11)$$

where $B \,\&\, C$ are viscosity enhancement coefficients. Thermophysical properties of water and nanoparticles are mentioned in Table 1.

The values of viscosity enhancement coefficients $B \,\&\, C$ for different shapes of nanoparticles are mentioned in Table 2.

### 2.6 Nondimensionalization

#### *2.6.1 Uniform Heating Condition*

The transformations used

$$\left.\begin{aligned} u = \frac{xU_0}{l}f'(\eta),\ v = -\frac{a}{r}\sqrt{\frac{\upsilon_f U_0}{l}}f(\eta), \\ \theta(\eta) = \frac{T-T_\infty}{T_w-T_\infty}, \eta = \frac{r^2-a^2}{2a}\sqrt{\frac{U_0}{\upsilon_f l}} \end{aligned}\right\} \quad \ldots (12)$$

Table 1 — Thermophysical properties of water and nanoparticles at 300K[23-25]

| | $\rho\left(kgm^{-3}\right)$ | $C_p\ (J/kgK)$ | $k\left(W/mK\right)$ | $\beta\left(\frac{1}{K}\right)$ | $\mu\left(Pa.s\right)$ | Shape |
|---|---|---|---|---|---|---|
| Water | 997.1 | 4179 | 0.613 | 0.00021 | 0.000909 | - |
| Ag (nanoparticle 1) | 10500 | 235 | 429 | $6.16\times10^{-5}$ | - | Spherical |
| $Al_2O_3$ (nanoparticle 2) | 3970 | 773 | 40 | $0.85\times10^{-5}$ | - | Spherical |
| Graphene (nanoparticle 3) | 2200 | 790 | 5000 | $-7\times10^{-6}$ | - | Platelets |

***2.6.2 Low Porosity Porous Media (Packed Bed of Small Particles)***

Using Eqs. (6) – (12), Eqs. (2 (a)) and (2 (b)) become

$$\frac{1}{\varepsilon}\frac{\mu_{THNF}}{\mu_f}\frac{\rho_f}{\rho_{THNF}}\left[(1+2\eta\Omega)f'''+\Omega f''\right]-\frac{1}{\varepsilon^2}\left[(f')^2-ff''\right]+\frac{\beta_{THNF}}{\beta_f}\left(\frac{Gr^*}{Da\,\mathrm{Re}^2}\right)\theta-\frac{\mu_{THNF}}{\mu_f}\frac{\rho_f}{\rho_{THNF}}\frac{\Lambda}{Da\,\mathrm{Re}}f'=0 \quad \text{... (13 (a))}$$

$$\left(\frac{k_{THNF}}{k_f}+\frac{4}{3Rd}\right)\frac{(\rho C_p)_f}{(\rho C_p)_{THNF}}\left[(1+2\eta\Omega)\theta''+\Omega\theta'\right]+\mathrm{Pr}\,f\theta'+\frac{(\mu)_{THNF}}{(\mu)_f}\frac{(\rho C_p)_f}{(\rho C_p)_{THNF}}\Lambda^2 Br\left[(1+2\eta\Omega)(f'')^2+\frac{\Lambda}{\mathrm{Re}\,Da}(f')^2\right]=0 \quad \text{... (13 (b))}$$

**2.7 High Porosity Porous Media (Metal Foam)**

Using Eqs. (6) – (12), Eqs. (3 (a)) and (3 (b)) become

$$\frac{1}{\varepsilon}\frac{\mu_{THNF}}{\mu_f}\frac{\rho_f}{\rho_{THNF}}\left[(1+2\eta\Omega)f'''+\Omega f''\right]-\frac{1}{\varepsilon^2}\left[(f')^2-ff''\right]+\frac{\beta_{THNF}}{\beta_f}\left(\frac{Gr^*}{Da\,\mathrm{Re}^2}\right)\theta-\frac{\mu_{THNF}}{\mu_f}\frac{\rho_f}{\rho_{THNF}}\frac{\Lambda}{Da\,\mathrm{Re}}f'-F_r(f')^2=0 \quad \text{... (14 (a))}$$

$$\left(\frac{k_{THNF}}{k_f}+\frac{4}{3Rd}\right)\frac{(\rho C_p)_f}{(\rho C_p)_{THNF}}\left[(1+2\eta\Omega)\theta''+\Omega\theta'\right]+\mathrm{Pr}\,f\theta'+\frac{(\mu)_{THNF}}{(\mu)_f}\frac{(\rho C_p)_f}{(\rho C_p)_{THNF}}\Lambda^2 Br\left[\begin{matrix}(1+2\eta\Omega)(f'')^2\\+\frac{\Lambda}{\mathrm{Re}\,Da}(f')^2\end{matrix}\right]+\frac{(\rho)_{THNF}}{(\rho)_f}\frac{(\rho C_p)_f}{(\rho C_p)_{THNF}}\Lambda^2 BrF_r(f')^3=0 \quad \text{… (14 (b))}$$

Table 2 — Values of viscosity enhancement coefficients $B$ & $C$ for different shapes of nanoparticles[24]

| Shape of nanoparticles | B | C | m |
|---|---|---|---|
| Platelets | 37.1 | 612.6 | 5.7 |
| Cylindrical | 13.5 | 904.4 | 4.9 |
| Spherical | 2.5 | 6.2 | 3 |

**2.8 Nondimensionalization of Boundary Conditions**

$$\left.\begin{aligned}f'(0)&=1+\frac{\gamma\left[f''(0)\mathrm{Re}^*f'(0)\right]}{\left[1-\delta\left\{f''(0)-\mathrm{Re}^*f'(0)\right\}\right]^{\frac{1}{2}}},\\ f(0)&=0,\theta(0)=1,\\ f'(\infty)&=0,\theta(\infty)=0\end{aligned}\right\} \quad \text{... (15)}$$

$$\left.\begin{aligned}&\mathrm{Re}_x=\frac{U_0x}{\upsilon_f},\Omega=\sqrt{\frac{l\upsilon_f}{U_0a^2}},F_r=Fx,Da=\frac{K}{l^2},G_r^*=\frac{g\beta_f\,\Delta T\,K\,\mathrm{Re}_x}{U_0\upsilon_f},\\ &\Lambda=\frac{x}{l},Rd=\frac{k^*k_f}{4\sigma^*T_\infty^3},\mathrm{Pr}=\frac{\upsilon_f}{\alpha_f},E_c=\frac{U_0^2}{\Delta T(C_p)_f},Br=\mathrm{Pr}.Ec\\ &\gamma=\gamma^*\frac{r}{a}\sqrt{\frac{U_0}{\upsilon_f l}},\mathrm{Re}^*=\mathrm{Re}^{-\frac{1}{2}}\left(\frac{al}{r^2}\right),\delta=\delta^*\frac{xU_0}{l}\frac{r}{a}\sqrt{\frac{U_0}{\upsilon_f l}}\end{aligned}\right\} \quad \text{… (16))}$$

are respectively Reynolds number, Curvature parameter, Forchheimer number, modified Darcy number, modified Grashof number, ratio parameter, radiation parameter, Prandtl number, Eckert number, Brinkman number, velocity slip parameter, modified Reynolds number, and non-dimensional critical shear rate. In addition, $\Delta T=T_w-T_\infty$ is the temperature difference parameter.

***2.8.1 Linear Heating Condition***

The transformations used

$$\left.\begin{aligned}&u=\frac{xU_0}{l}f'(\eta),\ v=-\frac{a}{r}\sqrt{\frac{\upsilon_fU_0}{l}}f(\eta),\\ &T=T_w=T_\infty+E\,a\,x\,\theta(\eta),\eta=\frac{r^2-a^2}{2a}\sqrt{\frac{U_0}{\upsilon_f l}}\end{aligned}\right\} \quad \text{… (17)}$$

#### *2.8.2 Low Porosity Porous Media (Packed Bed of Small Particles)*

Using Eqs. (6) – (11) and (17), Eqs. (2 (a)) and (2(b)) become

$$\frac{1}{\varepsilon}\frac{\mu_{THNF}}{\mu_f}\frac{\rho_f}{\rho_{THNF}}\left[(1+2\eta\Omega)f'''+\Omega f''\right]-\frac{1}{\varepsilon^2}\left[(f')^2-ff''\right]+\frac{\beta_{THNF}}{\beta_f}\left(\frac{Gr^*}{Da\,\mathrm{Re}^2\,\Lambda^2}\right)\theta-\frac{\mu_{THNF}}{\mu_f}\frac{\rho_f}{\rho_{THNF}}\frac{\Lambda}{Da\,\mathrm{Re}}f'=0 \quad \text{... (18 (a))}$$

$$\left(\frac{k_{THNF}}{k_f}+\frac{4}{3Rd}\right)\frac{(\rho C_p)_f}{(\rho C_p)_{THNF}}\left[(1+2\eta\Omega)\theta''+\Omega\theta'\right]+\mathrm{Pr}\left(f\theta'-f'\theta\right)+\frac{(\mu)_{THNF}}{(\mu)_f}\frac{(\rho C_p)_f}{(\rho C_p)_{THNF}}\Lambda^2 Br\left[\begin{matrix}(1+2\eta\Omega)(f'')^2\\+\frac{\Lambda}{\mathrm{Re}\,Da}(f')^2\end{matrix}\right]=0 \quad \text{… (18 (b))}$$

#### *2.8.3 High Porosity Porous Media (Metal Foam)*

Using Eqs. (6) – (11) and (17), Eqs. (3 (a)) and (3 (b)) become

$$\frac{1}{\varepsilon}\frac{\mu_{THNF}}{\mu_f}\frac{\rho_f}{\rho_{THNF}}\left[(1+2\eta\Omega)f'''+\Omega f''\right]-\frac{1}{\varepsilon^2}\left[(f')^2-ff''\right]+\frac{\beta_{THNF}}{\beta_f}\left(\frac{Gr^*}{Da\,\mathrm{Re}^2\,\Lambda^2}\right)\theta-\frac{\mu_{THNF}}{\mu_f}\frac{\rho_f}{\rho_{THNF}}\frac{\Lambda}{Da\,\mathrm{Re}}f'-F_r\left(f'\right)^2=0 \quad \text{... (19 (a))}$$

$$\left(\frac{k_{THNF}}{k_f}+\frac{4}{3Rd}\right)\frac{(\rho C_p)_f}{(\rho C_p)_{THNF}}\left[(1+2\eta\Omega)\theta''+\Omega\theta'\right]+\mathrm{Pr}\left(f\theta'-f'\theta\right)+\frac{(\mu)_{THNF}}{(\mu)_f}\frac{(\rho C_p)_f}{(\rho C_p)_{THNF}}\Lambda^2 Br\left[\begin{matrix}(1+2\eta\Omega)(f'')^2\\+\frac{\Lambda}{\mathrm{Re}\,Da}(f')^2\end{matrix}\right]+\frac{(\rho)_{THNF}}{(\rho)_f}\frac{(\rho C_p)_f}{(\rho C_p)_{THNF}}\Lambda^2 BrF_r(f')^3=0 \quad \text{… (19 (b))}$$

### 2.9 Nondimensionalization of Boundary Conditions

$$\left.\begin{aligned}f'(0)=1+\frac{\gamma\left[f''(0)-\Gamma f'(0)\right]}{\left[1-\delta\left\{f''(0)-\Gamma f'(0)\right\}\right]^{\frac{1}{2}}},\\ f(0)=0,\theta(0)=1,\\ f'(\infty)=0,\theta(\infty)=0\end{aligned}\right\} \quad \text{... (20)}$$

#### *2.9.1 Quantity of Great Importance*

The local skin friction coefficient and local Nusselt number

$$\mathrm{Re}_x^{0.5}\,C_f=-\frac{1}{\varepsilon}\frac{\mu_{THNF}}{\mu_f}f''(0) \quad \text{... (21)}$$

$$\left(\mathrm{Re}_x^{-0.5}\,Nu\right)_{UHBC}=-\Lambda\left(\frac{k_{THNF}}{k_f}+\frac{4}{3Rd}\right)\theta'(0) \quad \text{... (22)}$$

$$\left(\mathrm{Re}_x^{-0.5}\,Nu\right)_{LHBC}=-\frac{\Lambda}{\Omega}\left(\frac{k_{THNF}}{k_f}+\frac{4}{3Rd}\right)\theta'(0) \quad \text{... (23)}$$

## 3 Numerical Procedure

The Galerkin finite element method is implemented to resolve the reduced leading Eqs. (13)- (14) with the help of boundary condition (15) for the uniform heating condition, and (18)- (19) with the help of boundary condition (20) for the linear heating condition. Further, with the help of Picard's linearization approach, the nonlinear equations can be developed. Nonlinear equations are simulated with computational tolerance $10^{-5}$ with criteria $\left|\frac{x_{i+1}-x_i}{x_i}\right|<10^{-5}$.

## 4 Results and Discussion

### 4.1 Flow and Thermal Behavior of HNF and THNF in Low and High Porosity Porous Media Subject to Uniform and Linear Heating with Low Reynolds Numbers

#### *4.1.1 Flow Behavior of THNF and HNF in Low Porosity Porous Medium (Packed Bed of Small Particles)*

The flow behavior of axial velocity $f'(\eta)$ of THNF and HNF for disparate curvature parameter $\Omega\,(\Omega=0.1,0.2)$ at low Reynolds number $\mathrm{Re}$ $(\mathrm{Re}=0.2,0.3)$ with uniform heating conditions in low porous medium $(\varepsilon=0.1)$ is exhibited in Fig. 3. It is visualized that $f'(\eta)$ of THNF and HNF ameliorates with rise in $\Omega$ (from 0.1 to 0.2) at low Reynolds number $(\mathrm{Re}=0.2)$ subject to uniform heating. The radius of the curved sheet falls as the curvature parameter increases, indicating that the sheet becomes more curved. Compared to a flatter surface, a more curved surface provides less resistance to the fluid particles, enabling the nanofluid to travel more

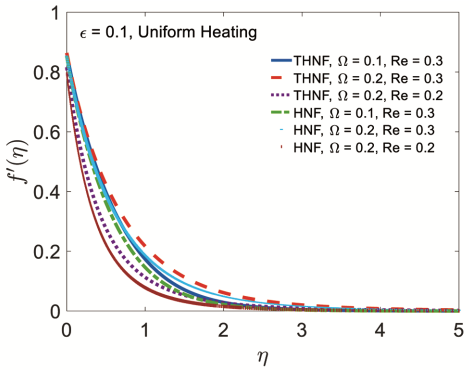


Fig. 3 — Illustration of $f'(\eta) vs\, \eta$ for different $\Omega$ and low Re for THNF and HNF subject to uniform heating and low porosity porous medium $(\varepsilon = 0.1)$

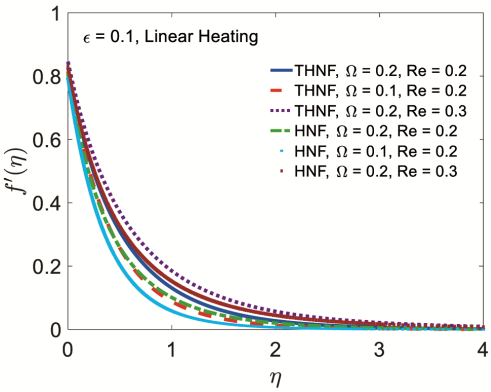


Fig. 4 — Illustration of $f'(\eta) vs\, \eta$ for different $\Omega$ and low Re for THNF and HNF subject to linear heating and low porosity porous medium $(\varepsilon = 0.1)$

quickly. Additionally, in packed beds where frictional loss is considerable, larger curvature decreases the overall area of the boundary in direct contact with the fluid, reducing the drag forces and enabling an improvement in the velocity profiles. Consequently, the velocity of THNF and HNF fluid upsurges. It is further visualized that amplification of Re $(\mathrm{Re} = 0.2, 0.3)$ emaciates $f'(\eta)$ of THNF and HNF at $\Omega = 0.1$. In a packed bed of small particles (low porosity), the fluid is forced through narrow, paths. As Re increases, inertial drag dominates over viscous forces within the complex, restricted flow path. It is understood from Fig. 4 that $f'(\eta)$ of both THNF and HNF intensifies when $\Omega$ rises from 0.1 to 0.3 at low Reynolds number $(\mathrm{Re} = 0.2)$ in low porosity porous medium subject to linear heating. However, $f'(\eta)$ exhibits reverse trend in linear heating condition.

As noticed in Fig. 5, $f'(\eta)$ of both THNF and HNF whittles down due to rise in $\gamma$ $(\gamma = 0.5, 1)$ at low

Reynolds number Re $(\mathrm{Re} = 0.2, 0.3)$ in uniform heating case of low porosity porous medium. This is because the surface can no longer fully transfer its momentum (stretching force) to the fluid. Further, $f'(\eta)$ of both THNF and HNF shows descending trend with increase of Re from 0.2 to 0.3. Exactly same behavior of $f'(\eta)$ is seen subject to linear heating (Fig. 6).

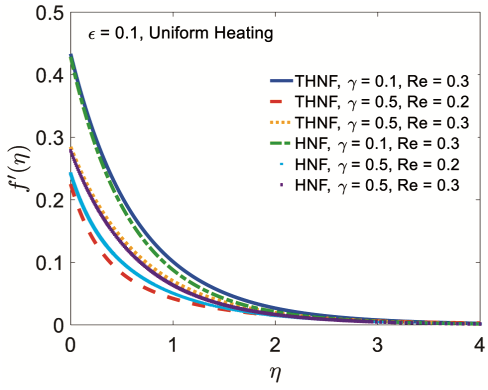


Fig. 5 — $f'(\eta) vs\, \eta$ for different $\gamma$ and low Re for THNF and HNF subject to uniform heating and low porosity porous medium $(\varepsilon = 0.1)$

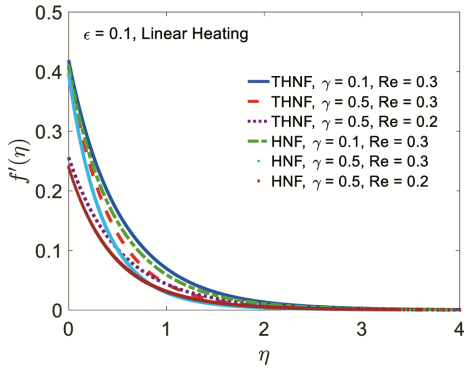


Fig. 6 — $f'(\eta) vs\, \eta$ for different $\gamma$ and low Re for THNF and HNF subject to linear heating and low porosity porous medium $(\varepsilon = 0.1)$

#### *4.1.2 Thermal Behavior of THNF and HNF in Low Porosity Medium (Packed Bed of Small Particles) with low Reynolds Numbers*

As portrayed in Fig. 7, fluid temperature $\theta(\eta)$ and the associated thermal boundary layer thickness (TBLT) of THNF and HNF enhance with rise in $\Omega$ with uniform heating. Near the wall, the ternary hybrid nano fluid's velocity increases due to the reduced surface resistance; this acceleration, along with the ternary nano particles' dense nature, raises the fluid particles' kinetic energy.

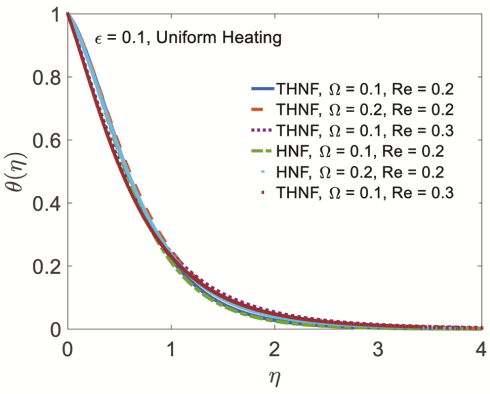


Fig. 7 — $\theta(\eta) vs\, \eta$ for different $\Omega$ and low $\mathrm{Re}$ for THNF and HNF subject to uniform heating and low porosity porous medium $(\varepsilon = 0.1)$

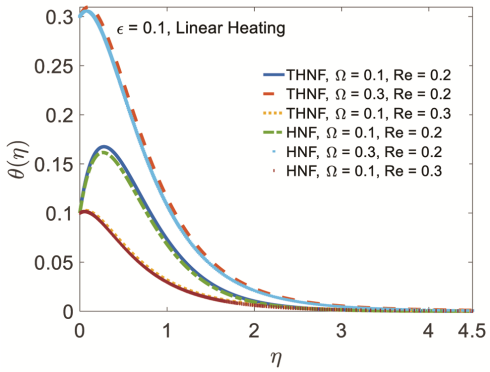


Fig. 8 — $\theta(\eta) vs\, \eta$ for different $\Omega$ and low Re for THNF and HNF subject to linear heating and low porosity porous medium $(\varepsilon = 0.1)$

Consequently, the temperature augments. Further, at fixed $\Omega$ (say, $\Omega = 0.1$), $\theta(\eta)$ decreases with increment in $\mathrm{Re}$ $(\mathrm{Re} = 0.2, 0.3)$ influenced by uniform boundary heating. It is visualized from Fig. 8 that $\theta(\eta)$ and its associated TBL of THNF and HNF grow prominently with rise in $\Omega$ $(\Omega = 0.1, 0.3)$ at low Reynolds number $(\mathrm{Re} = 0.2)$ under linear boundary heating condition. Moreover, $\theta(\eta)$ belittles significantly with rise in Reynolds number $(\mathrm{Re} = 0.2, 0.3)$ subject to linear heating. Appearance of temperature overshoots near the stretched boundary of the cylinder implicates that $\theta(\eta)$ is higher near the boundary than that towards the ambient.

#### *4.1.3 Flow Behavior of THNF and HNF in High Porosity Porous Medium (Metal Foam)*

Amplification of $F_r$ $(F_r = 0.2, 1)$ leads to the diminution in $f'(\eta)$ of THNF as well as HNF at low

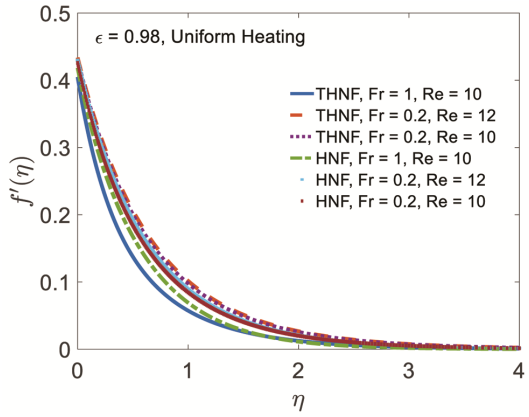


Fig. 9 — $f'(\eta) vs\, \eta$ for different $Fr$ and low $\mathrm{Re}$ for THNF and HNF subject to uniform heating and high porosity porous medium $(\varepsilon = 0.98)$

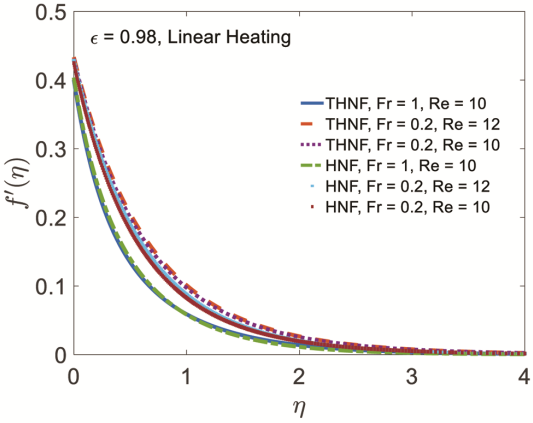


Fig. 10 — $f'(\eta) vs\, \eta$ for different $Fr$ and low $\mathrm{Re}$ for THNF and HNF subject to linear heating and high porosity porous medium $(\varepsilon = 0.98)$

$\mathrm{Re}$ subject to uniform heating in high porosity porous medium (Fig. 9). A quadratic dependence on velocity is introduced by the Forchheimer term. As this term rises, increasing pressure drops and decreased fluid speed result from the porous structure's increasing resistance to the flow. Metal foams have a complex interconnected structure, even when their porosity is large. The ternary hybrid nanofluid is slowed down by higher values of Forchheimer term because of increased inertial drag within its intricate internal geometry. Exactly same trend of $f'(\eta)$ for both THNF and HNF due to rise in Reynolds number $(\mathrm{Re} = 10, 12)$ subject to uniform heating is achieved. Further, same nature of $f'(\eta)$ is observed for both THNF and HNF with rise in $F_r$ in high porosity porous medium

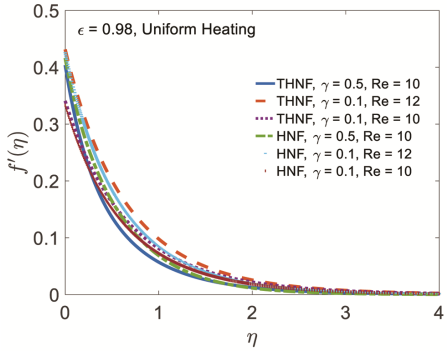


Fig. 11 —f $f'(\eta) vs\, \eta$ or different $\gamma$ and low $\mathrm{Re}$ for THNF and HNF subject to uniform heating and high porosity porous medium $(\varepsilon = 0.98)$

subject to linear heating (Fig. 10). Further, Fig. 11 indicates that rise in $\gamma$ $(\gamma = 0.1, 0.5)$ yields emaciation of $f'(\eta)$ for the THNF and HNF subject to uniform heating in foam materials. Because the larger slip permits a more substantial reduction in momentum transfer between the solid boundary and the fluid, a rise in the velocity slip parameter frequently results in a decrease in fluid velocity. The overall velocity in the boundary layer may decrease due to a slower velocity decay caused by the nonlinear character of the slip, which is frequently associated with high-order interactions or the porous matrix structure. Exactly similar behavior of $f'(\eta)$ for both THNF and HNF at fixed $\gamma$ $(\gamma = 0.1)$ and $\mathrm{Re}$ $(\mathrm{Re} = 10)$ subject to linear heating is visualized (Fig. 12).

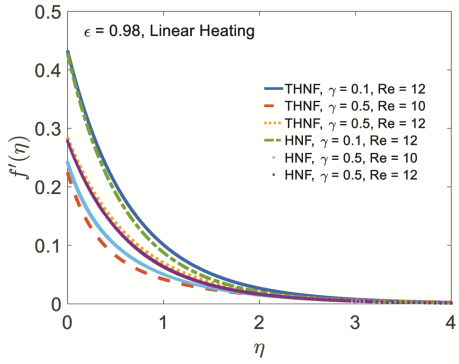


Fig. 12 — $f'(\eta) vs\, \eta$ for different $\gamma$ and low $\mathrm{Re}$ for THNF and HNF subject to linear heating and high porosity porous medium $(\varepsilon = 0.98)$

#### *4.1.4 Thermal Behavior of THNF and HNF in High Porosity Medium (Metal Foam)*

Figure 13 portrays the $\theta(\eta)$ behavior for different $\Omega$ at low Reynolds number $\mathrm{Re}$ $(\mathrm{Re} = 10, 12)$ subject to uniform boundary heating. It is seen that rise in $\Omega$ $(\Omega = 0.1, 0.3)$ leads to rise in $\theta(\eta)$ and the corresponding BLT escalation for both THNF and HNF subject to uniform heating. The boundary layer's curvature rises in tandem with the surface curvature, compelling the flow to take a more curved route. This increases the thickness of the boundary layer, which raises the fluid temperature and increases thermal resistance close to the surface. Diminution of $\theta(\eta)$ is envisaged for rise in Re Physically, rise in $\mathrm{Re}$ increases the velocity of THNF. The THNF moves through the heated metal foam more quickly as the flow velocity rises, reducing the amount of time that heat exchange occurs per unit volume of fluid. As a

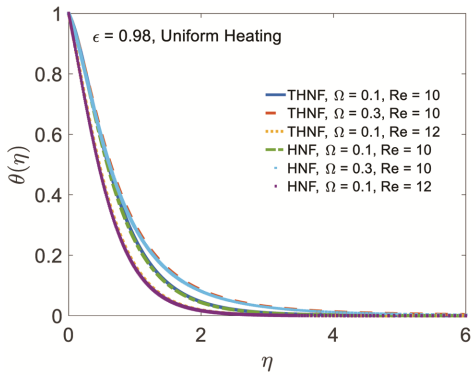


Fig. 13 — $\theta(\eta) vs\, \eta$ for different $\Omega$ and low $\mathrm{Re}$ for THNF and HNF subject to uniform heating and high porosity porous medium $(\varepsilon = 0.98)$

result, the exit temperature drops because the fluid does not remain in touch with the heated surface long enough to reach a higher temperature. In addition, $\theta(\eta)$ of THNF and HNF exhibit the same trend with amplification of $\Omega$ at low Reynolds number $\mathrm{Re}$ subject to linear boundary heating (Fig. 14).

### 4.2 Behavior of Skin Friction of and Nusselt Number (Heat Transfer Rate) of THNF Flow in Low Porosity Porous Medium Subject to Uniform and Linear Heating

As observed, from Fig. 15, increase in $\gamma$ ameliorates $C_f$ at each value of $Br$ for THNF flows under the influence of uniform boundary heating. The fluid is subjected to resistive (Darcy) and inertial (Forchheimer) drag forces by the porous structure (metal foam). In order to overcome the structural resistance, the velocity slip often increases the surface drag (skin friction), changing how the boundary layer forms in this high-drag environment.

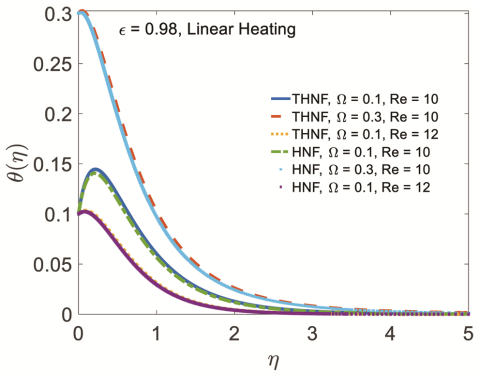


Fig. 14 — $\theta(\eta) vs\, \eta$ for different $\Omega$ and low $\mathrm{Re}$ for THNF and HNF subject to linear heating and high porosity porous medium $(\varepsilon = 0.98)$

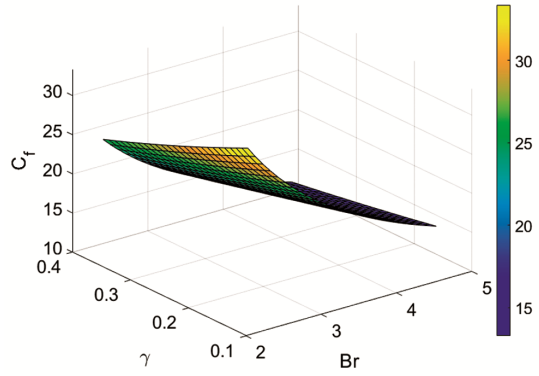


Fig. 15 — Variation of Skin friction $C_f$ with $Br$ and $\gamma$ for THNF subject to uniform heating in low porosity porous medium

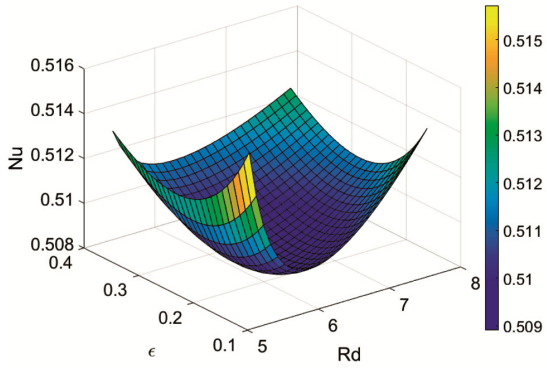


Fig. 16 — Variation of Nusselt number $Nu$ with $Rd$ and $\varepsilon$ for THNF subject to uniform heating in low porosity porous medium

As acknowledged from Fig. 16, rise in porosity parameter $\varepsilon$ escalates the values of HTR at each radiation parameter $Rd$ due to the flow of THNF subject to uniform boundary heating conditions. In high-porosity medium like metal foam, an increase in porosity typically raises the Nusselt number despite a decrease in total surface area because it significantly reduces the flow resistance, enabling higher flow velocity and higher mass flow rates through the porous structure. This higher velocity predominates in THNF (three distinct nanoparticles) in a nonlinear slip flow, offering better convective heat transmission. Further, faster heat transfer from the surface is made possible by increased radiation, which also reduces the viscosity effect and thins the thermal boundary layer.

## 5 Conclusion

The non-linear slip flow and thermal management of $Ag + Al_2O_3 + Graphene + Water$ THNF over a stretched cylinder in low porosity porous media (packed bed of small particles) and high porosity porous media (metal foam) subject to uniform and linear boundary heating conditions are investigated. The major outcomes of the present work are as follows:

i. As visualized, $f'(\eta)$ of THNF and HNF ameliorates with rise in $\Omega$ while it whittles down with rise in $\gamma$ at low Reynolds number subject to uniform and linear heating in low porosity porous media (packed bed of small particles) and high porosity porous media (metal foam).

ii. As analyzed, amplification of Reynolds number peters out $f'(\eta)$ of THNF and HNF subject to uniform and linear heating in both type of porous media considered.

iii. It is observed that $f'(\eta)$ is greater in linear heating case than uniform heating case.

iv. As expected, $\theta(\eta)$ and the associated thermal boundary layer thickness of THNF and HNF ameliorate with rise in $\Omega$, while reverse trend is attained with rise in $\gamma$ subject to uniform and linear heating in both type of porous media considered.

v. Augmentation of surface viscous drag (skin friction coefficient) is attained due to increase in $\gamma$ at different values of $Br$ $(1 \le Br \le 5)$ with uniform and linear boundary heating.

vi. Amelioration of HTR for THNF takes place from stretched cylinder thereby imparting significantly greater cooling due to increase in $\varepsilon$ at different values of $Rd$ $(5 \le Rd \le 8)$ subject to both type of boundary heating.

## Appendix

### Derivation of Eqs. 13 (a) and 13 (b)

Similarity Transformation

$$u=\frac{xu_0}{l}f'(\eta),\ v=-\frac{a}{r}\sqrt{\frac{\nu_f u_0}{l}}f(\eta),$$

$$\theta(\eta)=\frac{T-T_\infty}{T_w-T_\infty},\ \eta=\frac{r^2-a^2}{2a}\sqrt{\frac{u_0}{\nu_f l}}$$

### Momentum Equation

$$\frac{\rho_{THNF}}{\epsilon^2}\left(u\frac{\partial u}{\partial x}+v\frac{\partial u}{\partial r}\right)=\frac{\mu_{THNF}}{\epsilon}\left(\frac{\partial^2 u}{\partial r^2}+\frac{1}{r}\frac{\partial u}{\partial r}\right)+$$

$$g\rho_{THNF}\beta_{THNF}(T-T_\infty)-\frac{\mu_{THNF}u}{K}$$

Now,

$$\frac{\partial u}{\partial x}=\frac{u_0}{l}f',u\frac{\partial u}{\partial x}=\frac{{u_0}^2 x}{l^2}f'^2,$$

$$\frac{\partial u}{\partial r}=\frac{xu_0}{l}f''\cdot\frac{r}{a}\sqrt{\frac{u_0}{\nu_f l}},\ v\frac{\partial u}{\partial r}=-\frac{x{u_0}^2}{l}ff'',$$

$$\frac{\partial^2 u}{\partial r^2}=\frac{{u_0}^2 x}{\nu_f l^2}f'''\cdot\frac{r^2}{a^2},\ \frac{1}{r}\frac{\partial u}{\partial r}=\frac{xu_0}{l}f''\cdot\frac{1}{a}\sqrt{\frac{u_0}{\nu_f l}}$$

$$\therefore\frac{1}{\epsilon^2}\left(\frac{{u_0}^2 x}{l^2}f'^2-\frac{x{u_0}^2}{l^2}ff''\right)=\frac{1}{\epsilon}\left(\frac{\mu_{THNF}}{\mu_f}\right)\frac{\mu_f}{\left(\frac{\rho_{THNF}}{\rho_f}\right)\rho_f}\left(\begin{matrix}\frac{x{u_0}^2 r^2}{l^2a^2\nu_f}f'''+\\ \frac{x}{a}\frac{u_0}{l}\sqrt{\frac{u_0}{\nu_f l}}f''\end{matrix}\right)$$

$$+g\left(\frac{\beta_{THNF}}{\beta_f}\right)\beta_f(T_w-T_\infty)\theta-\left(\frac{\mu_{THNF}}{\mu_f}\right)\frac{\mu_f}{\left(\frac{\rho_{THNF}}{\rho_f}\right)\rho_f}\frac{u}{K}$$

$$\Rightarrow\frac{1}{\varepsilon}\frac{\mu_{THNF}}{\mu_f}\frac{\rho_f}{\rho_{THNF}}\left[(1+2\eta\Omega)f'''+\Omega f''\right]-$$

$$\frac{1}{\varepsilon^2}\left[(f')^2-ff''\right]+\frac{\beta_{THNF}}{\beta_f}\left(\frac{Gr^*}{Da\,\mathrm{Re}^2}\right)\theta-$$

$$\frac{\mu_{THNF}}{\mu_f}\frac{\rho_f}{\rho_{THNF}}\frac{\Lambda}{Da\,\mathrm{Re}}f'=0$$

### Temperature Equation

$$u\frac{\partial T}{\partial x}+v\frac{\partial T}{\partial r}=\left[\frac{k_{THNF}}{(\rho c_p)_{THNF}}+\frac{16\sigma^* T_\infty^3}{3k^*(\rho c_p)_{THNF}}\right]\left\{\begin{matrix}\frac{\partial^2 T}{dr^2}+\\ \frac{1}{r}\frac{\partial T}{dr}\end{matrix}\right\}$$

$$+\frac{\mu_{THNF}}{(\rho c_p)_{THNF}}\left(\frac{\partial u}{dr}\right)^2+\frac{\mu_{THNF}}{(\rho c_p)_{THNF}}\frac{u^2}{K}$$

$$\frac{\partial T}{dr}=(T_w-T_\infty)\theta'\cdot\frac{r}{a}\sqrt{\frac{U_0}{\nu_f l}},$$

$$v\frac{\partial T}{dr}=-(T_w-T_\infty)\frac{U_0}{l}f\theta'$$

$$\frac{\partial^2 T}{dr^2}=(T_w-T_\infty)\theta''\cdot\frac{r^2}{a^2}\left(\frac{U_0}{\nu_f l}\right),$$

$$\frac{1}{r}\frac{\partial T}{dr}=(T_w-T_\infty)\theta'\cdot\frac{1}{a}\sqrt{\frac{U_0}{\nu_f l}}$$

$$\therefore -f\theta'=\frac{1}{Pr}\left[\frac{k_{THNF}}{k_f}+\frac{4}{3Rd}\right]\frac{(\rho c_p)_f}{(\rho c_p)_{THNF}}\left[\begin{matrix}\frac{r^2}{a^2}\theta''+\\ \sqrt{\frac{l\nu_f}{aU_0}}\theta'\end{matrix}\right]$$

$$+\frac{\mu_{THNF}}{\mu_f}\cdot\frac{(\rho c_p)_f}{(\rho c_p)_{THNF}}\Lambda^2 Ec\left((1+2\eta\Omega)f''^2\right)+$$

$$\frac{\mu_{THNF}}{\mu_f}\cdot\frac{(\rho c_p)_f}{(\rho c_p)_{THNF}}\cdot\frac{\Lambda^2 Ec}{Da\,\mathrm{Re}}f'^2$$

$$\Rightarrow\left(\frac{k_{THNF}}{k_f}+\frac{4}{3Rd}\right)\frac{(\rho C_p)_f}{(\rho C_p)_{THNF}}\left[\begin{matrix}(1+2\eta\Omega)\theta''\\ +\Omega\theta'\end{matrix}\right]+\mathrm{Pr}\,f\theta'$$

$$+\frac{(\mu)_{THNF}}{(\mu)_f}\frac{(\rho C_p)_f}{(\rho C_p)_{THNF}}\Lambda^2 Br\left[\begin{matrix}(1+2\eta\Omega)(f'')^2+\\ \frac{\Lambda}{\mathrm{Re}\,Da}(f')^2\end{matrix}\right]=0$$

## References


1 Choi S U S & Eastman J A, (No.ANL/MSD/CP-84938. IL (United States): paper presented to the ASME International Mechanical Engineering Congress & Exposition, San Francisco, CA 12-17 November 1995.

2 Sa J & Nath G, *Indian J Pure Appl Phys*, 61 (2) (2023) 124.

3 Chaudhary S & Singh A, *Indian J Pure Appl Phys*, 61 (10) (2023) 830.

4 Sidik N A C, Yazid M N A W M & Mamat R, *Int Commun Heat Mass Transfer*, 68 (2015) 85.

5 Babu J R, Kumar K K & Rao S S, *Renew Sustain Energy Rev*, 77 (2017) 551.

6 Tamalapakula V B P, *Indian J Pure & Appl Phys*, 62 (5) (2024).

7 Barkathunnisa M, Chitra M & Rushi Kumar B, *Indian J Pure & Appl Phys*, 64 (4) (2026).

8 Sarangi M K, Thatoi D N, Nayak M K, Prakash J, Ramesh K & Azam M, *Int Commun Heat Mass Trans*, 138 (2022) 106337.

9 Elsaid F A E M, Alharthi T N, Eid M R & Emam T G, *Modern Phys Lett B*, 40 (8) (2026) 2650034.

10 Bejan A & Khair K R, *Int J Heat Mass Trans*, 28 (5) (1985) 902.

11 Alizadeh R, Abad J M N, Ameri A, Mohebbi M R, Mehdizadeh A, Zhao D & Karimi N, *J Taiwan Institute Chem Eng*, 124 (2021) 290.

12 Imran M, Hussain M, Jia W, Shah N A & Ali B, *Int Commun Heat and Mass Transfer*,169 (2025) 109761.

13 Deyi S, Mukhopadhaya S & Mandal M S, *Pramana J Phys*, 97 (66) (2023).

14 Mishra A, *Num Heat Transfer, Part B: Fundament*, 86 (8) (2025) 2640.

15 Gupta T, Panda A K & Kumar M, *Modern Phys Lett B*, 38 (02) (2024) 2350209.

16 Elsaid E M, Emam T G & Eid M R, *Heat Transfer*, 54 (7) (2025) 4723.

17 Batool K, Shakir S, Zainab S, Ahmad H, Alhubieshi N , Eid M R , Abd-Elmonem A & Almaliki A H , *Sci Reports,* 15 (2025) 34099.

18 Lal N D, Palanisamy S K, Paranthaman P, Sathishkumar A A N N & Kandasamy J**,** *Indian J Pure Appl Phys*, 64 (3) (2026).

19 Kashyap S, Sarkar J & Kumar A, *Energy*, 225 (2021) 120199.

20 Sahoo R R, *Powder Technol*, 370 (2020) 19.

21 Khan A, Hashim Farooq M, Hussain S M, Ahmad H, Jamshed W, Eid M R & Suoliman N A A, *J Radiat Res Appl Sci*, 18 (4) (2025) 101974.

22 Patil V S , Shamshuddin MD , Humane P P , Eid M R , Salawu S O, Alsemiry R D & Elsaid E M , *Modern Phys Lett B*, 39 (28) (2025) 2550137.

23 Shamshuddin MD **,** Saeed A **,** Mishra S R **,** Panda S **,** Alruwaili A S & Eid M R **,** *Modern Phys Lett B*, 39 (21) ( 2025) 2550061.

24 Adun H, Adedeji M, Dagbasi M & Babatunde A, *J Energy Storage*, 51 (2022) 104531.

25 Li Z, Shahsavar A, Niazi K, Al-Rashed A A A A & Rostami S, *Int Commun Heat Mass Transf*, 115 (2020) 104628.